Institute of Electronics, Information, and Communication Engineers

IEICE TRANS. COMMUN., VOL.E88–B, NO.6 JUNE 2005

PAPER Special Section on 2004 International Symposium on Antennas and Propagation

A Study on Polarimetric Correlation Coefficient for Feature Extraction of Polarimetric SAR Data

Toshifumi MORIYAMA[†a)], **Yoshio YAMAGUCHI**[††], **Seiho URATSUKA**[†], *Members*, **Toshihiko UMEHARA**[†], **Hideo MAENO**[†], *Nonmembers*, **Makoto SATAKE**[†], **Akitsugu NADAI**[†], *Members*, *and* **Kazuki NAKAMURA**[†], *Nonmember*

SUMMARY This paper attempts to use the polarimetric correlation coefficient for extraction of the polarimetric features of the urban areas and the natural distributed areas from Polarimetric Synthetic Aperture Radar (POLSAR) data. There is a possibility that the polarimetric correlation coefficient can reveal various scattering mechanisms of terrains based on the reflection symmetry property. In order to verify the capability of polarimetric correlation coefficient, we examined the behavior of this coefficient of the urban areas and the natural distributed areas with respect to the several polarimetric scattering models in the linear and circular polarization bases, and the difference of the polarimetric scattering characteristics between these two areas was derived. It was confirmed that the polarimetric correlation coefficient is useful to extract the polarimetric features from the actual L-band and X-band POLSAR data.

key words: *radar polarimetry, polarimetric correlation coefficient, urban areas, natural distributed areas, reflection symmetry*

1. Introduction

It is well known that the polarimetric information is useful for classification and segmentation in many terrains. Various analyses to Polarimetric Synthetic Aperture Radar (POLSAR) image have been carried out [1]–[3], [5], [7], [9], [10], [12]. The main purpose is to extract the polarimetric features from POLSAR data including both the amplitude and the phase. Among the various analyses, Polarimetric Entropy-Alpha (H-α) method [2] is the most popular technique to estimate the statistical polarimetric data. This technique assigns the statistical polarimetric data to eight zones in the H-α plane. Since the preset zone boundaries in the H-α plane often become unsuitable to the experimental data, there is a possibility that the urban areas are mixed with the natural distributed areas. The three-component scattering model [3] based on the reflection symmetry ($\langle S_{HH}S_{HV}^{*}\rangle = \langle S_{HV}S_{VV}^{*}\rangle = 0$, $\langle\cdot\rangle$ and the superscript * denote ensemble average and complex conjugate, respectively.) provided the excellent decomposition results of forest areas. Since the polarimetric scattering characteristics of the urban areas do not often satisfy the reflection symmetry ($\langle S_{HH}S_{HV}^{*}\rangle \neq 0$, $\langle S_{HV}S_{VV}^{*}\rangle \neq 0$), this decomposition technique cannot be applied to the urban areas. In addition, the polarimetric backscatter from the urban areas significantly changes with the orientation, shape and distributions of buildings, houses and street patterns. These effects influence other techniques using single polarimetric SAR data such as Neural network, Fuzzy, Maximum-likelihood approach, etc. [4], [5].

In this paper, the polarimetric correlation coefficient is examined to extract polarimetric features in the natural distributed areas and the urban areas in order to overcome above-mentioned problems. For extraction of the polarimetric features, it is expected to deal with statistics of POLSAR data such as averaged covariance, coherency and Mueller matrices. Since the elements of these matrices are related to the polarimetric correlation coefficient, it is important to analyze this coefficient concerning various specific areas. It is known that the polarimetric correlation coefficient is useful for estimating the surface roughness [6] and that the like-polarized correlation coefficient in the circular polarization basis indicates a dependence on the roughness state (by using the POLSAR data that observed the agricultural area). The same coefficient was shown to serve a discrimination of tree types experimentally [7]. On the other hand, this paper investigates the behavior of polarimetric correlation coefficient with respect to several physical polarimetric scattering models. This attempt gives us a theoretical interpretation of polarimetric correlation coefficient to the experimental data and can be used to design and develop robust classification algorithm of the POLSAR data. The physical scattering models for the natural distributed areas are based on the three-component scattering models (surface/double-bounce/volume scatterings) [3]. For the urban areas, two physical scattering models (odd(single and triple)-bounce/even(double)-bounce scatterings) are considered based on the high frequency technique [8]–[10]. The difference of physical scattering model in the natural distributed areas and the urban areas is related to the reflection symmetry. Moreover, in order to distinguish between the natural distributed areas and the urban areas, the variation of polarimetric correlation coefficient is examined not only in the linear polarization basis (HV) but also in the circular polarization basis (RL).

In Sect. 2, the relationship between the polarimetric statistical data and polarimetric correlation coefficient is described. In Sect. 3, the polarimetric scattering characteristics of the natural distributed areas and the urban areas are

Manuscript received October 1, 2004.
Manuscript revised January 7, 2005.

[†]The authors are with Environment Information Technology Group, Applied Research and Standards Department, National Institute of Information and Communications Technology, Koganei-shi, 184-8795 Japan.
[††]The author is with Department of Information Engineering, Niigata University, Niigata-shi, 950-2181 Japan.
a) E-mail: toshi.moriyama@nict.go.jp

DOI: 10.1093/ietcom/e88–b.6.2353

Copyright © 2005 The Institute of Electronics, Information and Communication Engineers

NII-Electronic Library Service

Institute of Electronics, Information, and Communication Engineers

briefly summarized. In Sect. 4, the polarimetric correlation coefficients are analyzed in the linear and circular polarization bases. Finally, the experimental results are given by using X-band and L-band of POLSAR data acquired by Pi-SAR [15]. It is confirmed that the polarimetric correlation coefficient is useful for feature extraction in the natural distributed areas and the urban areas.

2. Polarimetric Statistical Data and Polarimetric Correlation Coefficient

If the polarimetric measurement is conducted in the linear (HV) basis by the polarimetric synthetic aperture radar, the set of polarimetric scattering coefficients at each pixel of SAR image provides the scattering matrix

$$[S\,(HV)] = \begin{bmatrix} S_{HH} & S_{HV} \\ S_{VH} & S_{VV} \end{bmatrix}, \tag{1}$$

where the subscripts H and V refer to the horizontal and the vertical polarizations, respectively. For the reciprocal backscattering case, S_{HV} is identical with S_{VH}. In order to interpret scattering property in some specific areas, it is necessary to deal with the second order statistics of scattering matrix. The covariance matrix [1], [3] is suited to evaluate the statistical data. The covariance matrix $[C_i(HV)]$ for the ith pixel of POLSAR image is defined as

$$\boldsymbol{u}_i = \begin{bmatrix} S_{HH} & \sqrt{2}S_{HV} & S_{VV} \end{bmatrix}^T, \tag{2}$$

$$[C_i\,(HV)] = \boldsymbol{u}_i \boldsymbol{u}_i^{*T} = \begin{bmatrix} S_{HH}S_{HH}^* & \sqrt{2}S_{HH}S_{HV}^* & S_{HH}S_{VV}^* \\ \sqrt{2}S_{HV}S_{HH}^* & 2S_{HV}S_{HV}^* & \sqrt{2}S_{HV}S_{VV}^* \\ S_{VV}S_{HH}^* & \sqrt{2}S_{VV}S_{HV}^* & S_{VV}S_{VV}^* \end{bmatrix}, \tag{3}$$

where $\boldsymbol{u}$ and T are a target vector and transpose, respectively. The ensemble average covariance matrix $[\langle C(HV)\rangle]$ is obtained by averaging n neighboring pixels.

$$[\langle C\,(HV)\rangle] = \frac{1}{n}\sum_{i=1}^{n}[C_i\,(HV)] \tag{4}$$

$[\langle C(HV)\rangle]$ can be normalized by σ_{VV} and be written as [12]

$$[\langle C\,(HV)\rangle] = \sigma_{VV}\begin{bmatrix} g & \sqrt{2}\eta\sqrt{eg} & \gamma\sqrt{g} \\ \sqrt{2}\eta^*\sqrt{eg} & 2e & \sqrt{2}\zeta\sqrt{e} \\ \gamma^*\sqrt{g} & \sqrt{2}\zeta^*\sqrt{e} & 1 \end{bmatrix}, \tag{5}$$

$$\sigma_{VV} = \langle S_{VV}S_{VV}^*\rangle, \quad g = \frac{\langle S_{HH}S_{HH}^*\rangle}{\langle S_{VV}S_{VV}^*\rangle},$$

$$e = \frac{\langle S_{HV}S_{HV}^*\rangle}{\langle S_{VV}S_{VV}^*\rangle},$$

$$\gamma = Cor(HH,VV), \quad \eta = Cor(HH,HV), \quad \text{and } \zeta = Cor(HV,VV) \tag{6}$$

where $Cor(XY,AB)$ is a polarimetric correlation coefficient between XY and AB channels and is defined by [6]

$$Cor\,(XY,AB) = \frac{\langle S_{XY}S_{AB}^*\rangle}{\sqrt{\langle S_{XY}S_{XY}^*\rangle\langle S_{AB}S_{AB}^*\rangle}}. \tag{7}$$

Therefore, the polarimetric correlation coefficient is connected to each component of the covariance matrix directly, and plays an important role as representing the polarimetric features.

3. Scattering Characteristics of the Natural Distributed Areas and the Urban Areas

The various terrains (on the earth surface) are roughly divided into two categories. One is the natural distributed areas such as forests, moors, vegetable fields and the seas. The other is the urban areas which consist of man-made targets such as houses and buildings. The polarimetric scattering characteristics in these two areas are investigated in some literatures [3], [8]–[10]. The objective of the literatures is to build the scattering models for analytical evaluation of electromagnetic returns (the forward problem) and to retrieve the electromagnetic properties of targets from the radar signal (the inverse problem). These trials are very important to improve the analysis technique of remote sensing. For example, Durden and Freeman [3] suggested a decomposition technique based on the covariance matrix and the physical scattering model (surface/double-bounce/volume scatterings). Their approach is very useful for understanding of polarimetric scattering mechanisms in the natural distributed areas. Franceschetti, Iodice and Riccio [8] provided the canonical problems in the electromagnetic backscattering from the buildings. These results give us the knowledge of a polarimetric relationship between the radar responses and the urban structures. According to the literatures [3], [8], [10], the polarimetric scattering characteristics of the natural distributed areas and the urban areas are described as follows.

3.1 Natural Distributed Areas

An approach of Durden and Freeman's decomposition [3] serves for understanding of scattering mechanism in the natural distributed areas. Their decomposition divides the measured covariance matrix into three scattering mechanisms, i.e., surface, volume and double-bounce scatterings. These three mechanisms (as shown in Fig. 1(a)) are the dominant elements in the backscattering from forest areas and are assumed to satisfy the reflection symmetry as

$$\langle S_{HH}S_{HV}^*\rangle = \langle S_{HV}S_{VV}^*\rangle = 0. \tag{8}$$

The reflection symmetry is essentially related to a scattering from a random surface and a random layer media in space, and is very important characteristic for the natural distributed areas. The surface scattering component is modeled by the scattering from a first-order Bragg surface. The

NII-Electronic Library Service

Institute of Electronics, Information, and Communication Engineers

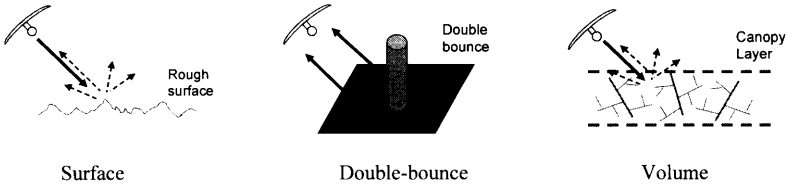

Surface Double-bounce Volume

(a) Natural distributed areas.

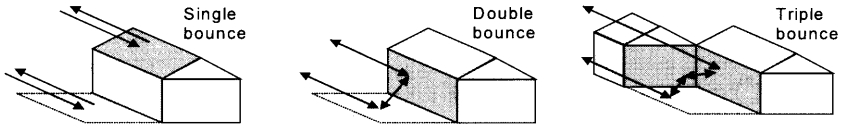

Single-bounce Double-bounce Triple-bounce

(b) Urban areas.

Fig. 1 The scattering model for each area.

double-bounce scattering component is formed by the scattering from a dihedral corner reflector which accounts for a ground-trunk interaction. The scattering matrixes and the second-order scattering statistics of surface and double-bounce scattering mechanisms are given by

• Surface scattering:

$$\left[S_{surface}(HV)\right] = \begin{bmatrix} \beta & 0 \\ 0 & 1 \end{bmatrix}, \mathrm{Re}(\beta) > 0 \tag{9a}$$

$$\left\langle |S_{HH}|^2 \right\rangle = \left\langle |\beta|^2 \right\rangle, \left\langle |S_{VV}|^2 \right\rangle = 1, \langle S_{HH} S_{VV}^* \rangle = \beta, \left\langle |S_{HV}|^2 \right\rangle = 0, \tag{9b}$$

and

$$\langle S_{HH} S_{HV}^* \rangle = \langle S_{HV} S_{VV}^* \rangle = 0,$$

• Double-bounce scattering:

$$[S_{double}(HV)] = \begin{bmatrix} \alpha & 0 \\ 0 & 1 \end{bmatrix}, \quad \mathrm{Re}(\alpha) < 0 \tag{10a}$$

$$\left\langle |S_{HH}|^2 \right\rangle = \left\langle |\alpha|^2 \right\rangle, \left\langle |S_{VV}|^2 \right\rangle = 1, \langle S_{HH} S_{VV}^* \rangle = \alpha, \left\langle |S_{HV}|^2 \right\rangle = 0, \tag{10b}$$

and

$$\langle S_{HH} S_{HV}^* \rangle = \langle S_{HV} S_{VV}^* \rangle = 0,$$

where β and α are a ratio of HH backscatter to VV backscatter (S_{HH}/S_{VV}) of surface and double-bounce mechanisms, respectively [3]. It is clear that the reflection symmetry is derived from Eqs. (9b), (10b). In the case of volume scattering, this mechanism is caused by the canopy which consists of many dipoles (such as leaves, twigs and branches) randomly oriented in azimuth direction. The scattering matrix of a dipole is written by [13]

$$\left[S_{dipole}(HV)\right] = \begin{bmatrix} \cos^2\theta & \sin\theta\cos\theta \\ \sin\theta\cos\theta & \sin^2\theta \end{bmatrix}, \tag{11}$$

where θ is an orientation angle in a plane orthogonal to radar line of sight. The distribution of dipole orientation angle can be determined by a probability density function $P(\theta)$. Based on the probability density function $P(\theta)$, the expected value $\langle F \rangle$ of any function $f(\theta)$ can be derived by [3]

$$\langle F \rangle = \int_0^{2\pi} d\theta f(\theta) P(\theta). \tag{12}$$

Therefore, by using Eq. (12), the theoretical second order scattering statistics of volume scattering are given by

• Volume scattering:

$$\left\langle |S_{HH}|^2 \right\rangle = \left\langle |S_{VV}|^2 \right\rangle = 1, \langle S_{HH} S_{VV}^* \rangle = \left\langle |S_{HV}|^2 \right\rangle = \frac{1}{3}, \tag{13}$$

and

$$\langle S_{HH} S_{HV}^* \rangle = \langle S_{HV} S_{VV}^* \rangle = 0,$$

where we assume that $P(\theta)$ is uniform. The volume scattering can be also related to the reflection symmetry.

3.2 Urban Areas

The urban areas are composed of many man-made targets such as houses and buildings. The radar cross section of man-made targets is calculated by coherently combining the reflected waves which are typically caused by single-, double- and triple-bounce scatterings as illustrated in Fig. 1(b) [8]–[10]. The scattering waves from the urban areas can be treated deterministically [11], because the man-made targets do not vary randomly in space. The single-bounce scattering is relevant to bare soil (rough ground), building roofs and vertical walls. The double-bounce scattering is caused by dihedral structures formed by vertical walls and the ground. The triple-bounce scattering is generated by trihedral structures formed by wall-ground-wall. The three scattering mechanisms can be classified into an odd- and an even-bounce scattering types. The single- and triple-bounce scattering mechanisms are considered as same

NII-Electronic Library Service

Institute of Electronics, Information, and Communication Engineers

scattering matrix (odd-bounce scattering type). The double-bounce scattering corresponds to an even-bounce scattering type. The scattering matrix and the second order scattering statistics with respect to each scattering type in urban areas can be written by

• Odd-bounce scattering:

$$[S_{odd}(HV)] = \begin{bmatrix} \beta' & 0 \\ 0 & 1 \end{bmatrix}, \ \mathrm{Re}(\beta') > 0 \tag{14a}$$

$$\langle |S_{HH}|^2 \rangle = \langle |\beta'|^2 \rangle, \ \langle |S_{VV}|^2 \rangle = 1,$$
$$\langle S_{HH} S_{VV}^* \rangle = \beta', \ \langle |S_{HV}|^2 \rangle = 0, \tag{14b}$$

and

$$\langle S_{HH} S_{HV}^* \rangle = \langle S_{HV} S_{VV}^* \rangle = 0,$$

• Even-bounce scattering:

$$[S_{even}(HV)] = \begin{bmatrix} \alpha' & \rho \\ \rho & 1 \end{bmatrix},$$
$$\mathrm{Re}(\alpha') < 0 \begin{cases} \rho = 0, (\phi = 0) \\ \rho \neq 0, (\phi \neq 0) \end{cases} \tag{15a}$$

$$\langle |S_{HH}|^2 \rangle = \langle |\alpha'|^2 \rangle, \ \langle |S_{VV}|^2 \rangle = 1,$$
$$\langle S_{HH} S_{VV}^* \rangle = \alpha', \ \langle |S_{HV}|^2 \rangle = |\rho|^2, \tag{15b}$$

and

$$\langle S_{HH} S_{HV}^* \rangle = \alpha' \rho^*, \ \langle S_{HV} S_{VV}^* \rangle = \rho,$$

where α' and β' are a ratio of HH backscatter to VV backscatter of each type, and ρ is a ratio of HV backscatter to VV backscatter of even-bounce scattering type. In the case of odd-bounce scattering type, this mechanism typically represents the specular reflection and does not provide the cross-polarized response. The trihedral corner reflector which is dominant source in this type has polarimetric characteristic which suppresses the cross-polarized response in wide angle area [14], and can be used for a calibration in like-polarized channel between HH and VV. On the other hand, we assume that the generation of a cross-polarized response is restricted to the even-bounce scattering type and depends on angle ϕ (ϕ is a street orientation angle as shown in Fig. 2), because the cross-polarized response appears except for the area where a road direction is parallel to the azimuth direction in the urban areas [8], [9]. Since the scattering waves from the urban areas occur deterministically, the polarimetric scattering quantity does not need a statistical processing for target orientation. Therefore, there is a possibility that the urban areas do not show the reflection symmetry

$$\langle S_{HH} S_{HV}^* \rangle = \alpha' \rho \neq 0, \langle S_{HV} S_{VV}^* \rangle = \rho \neq 0, \tag{16}$$

and the polarimetric scattering characteristics of urban areas is very different from that of the natural distributed areas.

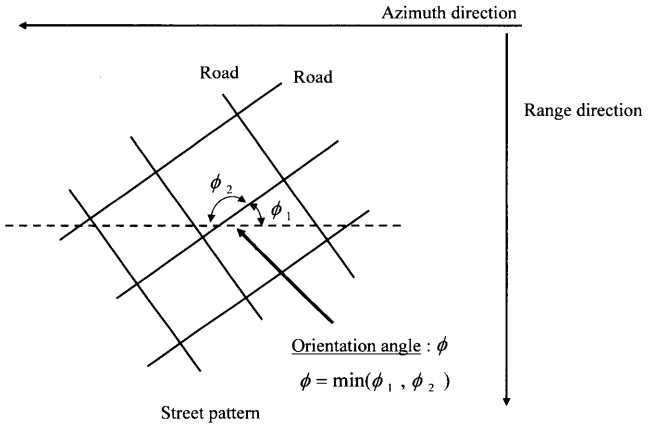

Fig. 2 The definition of orientation angle of street pattern.

4. Polarimetric Correlation Coefficient

By using the above-mentioned polarimetric scattering characteristics of the natural distributed areas and the urban areas, we examine the behavior of polarimetric correlation coefficient in the linear and circular polarization bases. The scattering matrix in the circular polarization basis (RL) can be transformed from that in the linear polarization basis (HV) by following equations as

$$\begin{cases} S_{RR} = (S_{HH} - S_{VV} - j2S_{HV})/2 \\ S_{LL} = (S_{VV} - S_{HH} - j2S_{HV})/2 \\ S_{RL} = S_{LR} = -j(S_{HH} + S_{VV})/2 \end{cases}, \tag{17}$$

where the subscripts R and L are the right and the left circular polarizations, respectively.

4.1 Linear Polarization Basis

The key point to extract the polarimetric characteristics from the natural distributed areas and the urban areas is the following properties as

$$\langle S_{HH} S_{HV}^* \rangle = \langle S_{HV} S_{VV}^* \rangle = 0$$
for natural distributed areas
$$\langle S_{HH} S_{HV}^* \rangle \neq 0, \ \langle S_{HV} S_{VV}^* \rangle \neq 0 \text{ for urban areas.}$$

Since various terrains in the natural distributed areas indicate a property of the reflection symmetry, the polarimetric correlation coefficient between like- and cross-polarized channels is close to zero. On the other hand, in the urban areas, one of the dominant scattering mechanisms is even-bounce scattering type whose matrix is expressed in Eq. (15). So, the even-bounce scattering type does not show the reflection symmetry. Therefore, it is expected that the magnitude of polarimetric correlation coefficient between the like- and cross-polarized channels in the urban areas is higher than that in the natural distributed areas. However, when a road direction is parallel to the azimuth direction, the difference between two areas does not appear significantly due to the dependence of the cross-polarized response with respect to a street orientation angle.

NII-Electronic Library Service

Institute of Electronics, Information, and Communication Engineers

4.2 Circular Polarization Basis

In circular polarization basis, there are two polarimetric correlation coefficients being considered for feature extraction. One is the coefficient between the like-polarized channels (*RR* and *LL*). The other is the coefficient between like- and cross-channels (*RR* and *RL* or *RL* and *LL*). We choose the former coefficient, because the like-polarized channels exhibit the clear difference of scattering characteristics between the natural distributed areas and the urban areas.

In the natural distributed areas except for sea areas, a volume scattering becomes a dominant mechanism in higher microwave frequencies above C-band. In order to evaluate the theoretical polarimetric correlation coefficient between *RR* and *LL* of volume scattering, it is necessary to calculate the quantity $\langle S_{RR}S_{LL}^* \rangle$ from Eqs. (11), (12) and (17). The scattering matrix of a dipole in circular polarization basis is

$$\left[S_{dipole}(RL)\right] = \frac{1}{2} \begin{bmatrix} \cos^2\theta - \sin^2\theta - j2\sin\theta\cos\theta & -j \\ -j & \sin^2\theta - \cos^2\theta - j2\sin\theta\cos\theta \end{bmatrix}. \tag{18}$$

The second order scattering statistic between *RR* and *LL* channels in volume scattering becomes

- Volume scattering:

$$\langle S_{RR}S_{LL}^* \rangle = 0, \tag{19}$$

where it is assumed that an orientation distribution of dipole is uniform. This effect expresses the polarimetric correlation coefficient between *RR* and *LL* is close to zero in the natural distributed areas. On the other hand, the odd- and even-bounce scattering types become the main scattering contributions in urban areas. A cross-correlation ($\langle S_{RR}S_{LL}^* \rangle$) of these two mechanisms can be transformed as follows:

- Odd-bounce scattering:

$$\begin{aligned} \langle S_{RR}S_{LL}^* \rangle &= -\langle S_{RR}S_{RR}^* \rangle = -\langle S_{LL}S_{LL}^* \rangle \\ &= -\left(|\beta'|^2 - \beta' - \beta'^* + 1\right)/4, \end{aligned} \tag{20}$$

- Even-bounce scattering:

$$\begin{aligned} \langle S_{RR}S_{LL}^* \rangle &= (\alpha' - 1 - j2\rho)(-\alpha'^* + 1 + j2\rho^*)/4, \\ \langle S_{RR}S_{RR}^* \rangle &= (\alpha' - 1 - j2\rho)(\alpha'^* - 1 + j2\rho^*)/4, \end{aligned} \tag{21}$$

and

$$\langle S_{LL}S_{LL}^* \rangle = (-\alpha' + 1 - j2\rho)(-\alpha'^* + 1 + j2\rho^*)/4.$$

We assume that the cross-polarized component ρ of the even-bounce scattering type is equal to zero, because the cross-polarized response is very small from the like polarized responses. Thus, $\langle S_{RR}S_{LL}^* \rangle$ of even-bounce scattering type can be simplified as

$$\begin{aligned} \langle S_{RR}S_{LL}^* \rangle &\approx -\langle S_{RR}S_{RR}^* \rangle = -\langle S_{LL}S_{LL}^* \rangle \\ &= -\left(|\alpha'|^2 - \alpha' - \alpha'^* + 1\right)/4. \end{aligned} \tag{22}$$

These results mean the magnitude of polarimetric correlation coefficient between *RR* and *LL* in the urban areas is close to one as follows,

$$\begin{aligned} Cor(RR, LL) &= \frac{\langle S_{RR}S_{LL}^* \rangle}{\sqrt{\langle S_{RR}S_{RR}^* \rangle \langle S_{LL}S_{LL}^* \rangle}} \\ &\approx \frac{\langle S_{RR}S_{LL}^* \rangle}{\sqrt{\langle S_{RR}S_{LL}^* \rangle \langle S_{RR}S_{LL}^* \rangle}} = 1. \end{aligned} \tag{23}$$

Then, it is predicted that the magnitude of polarimetric correlation coefficient between *RR* and *LL* in the urban areas is higher than that in the natural distributed areas. However, the coefficient in the urban areas decreases with increasing the street orientation angle ϕ.

Therefore, it is possible that the above-mentioned indices, i.e. $Cor(S_{HH}, S_{HV})$, $Cor(S_{HV}, S_{VV})$ and $Cor(S_{RR}, S_{LL})$, distinguish between the urban areas and the natural distributed areas. Some useful results of polarimetric correlation coefficient are summarized in Table 1.

Table 1 The behavior of polarimetric correlation coefficient.

	Natural distributed areas	Urban areas	
		$\phi \neq 0$	$\phi = 0$
$\lvert Cor(HH,HV)\rvert$, $\lvert Cor(HV,VV)\rvert$	Low	High	Low
	Reflection symmetry	Non reflection symmetry	
$\lvert Cor(RR,LL)\rvert$	Low	High	
	Volume scattering	Odd/even-bounce scatterings	

5. Experimental Results

In August 2003, an area around Kobari in Niigata, Japan was observed by NICT/JAXA's airborne polarimetric SAR system, known as Pi-SAR [15]. This data was chosen for examination of the polarimetric correlation coefficients ($Cor(S_{HH}, S_{HV})$, $Cor(S_{HV}, S_{VV})$ and $Cor(S_{RR}, S_{LL})$). The aerial photograph of the Kobari area is shown in Fig. 3. Figure 4 shows the observation results for X-band (3.14 cm) and L-band (23.6 cm). This image is assigned to the R GB colors with respect to each polarization state (*HH*: red, *HV*: green, *VV*: blue). The image size is 5 km by 5 km. The resolution (azimuth and slant range directions) is 1.5 m for the X-band and 3 m for the L-band. In the Kobari area, there are five categories, i.e., the sea areas, the pine woods areas, the vegetable field areas, rice paddy fields areas and urban areas. These five categories are used for evaluation of the polarimetric correlation coefficients. The each evaluated area of X-band is composed of 100 by 100 pixels blocked in Fig. 4(b) except for vegetable field area (40 by 40 pixels). The area of L-band is half size of X-band due to the difference of pixel size (1.25 m for X-band, 2.5 m for L-band). In advance data analysis, the filter to average the covariance matrix is applied to each band data in 15 by 15 window for

NII-Electronic Library Service

Institute of Electronics, Information, and Communication Engineers

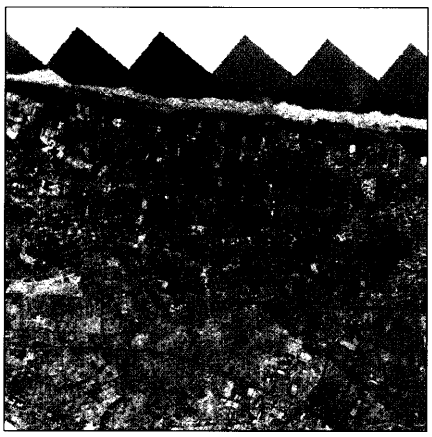

Fig. 3 The aerial photograph of the Kobari area in Niigata city.

X-band and 11 by 11 window for L-band.

The images of the three coefficients are shown in Fig. 5. The magnitude of averaged coefficient in each evaluated areas is listed in Tables 2(a), (b). The urban areas appear similarly at X-band and L-band and show high correlation. However, the area indexed by urban 2 in Fig. 4(b) where a road direction is parallel to the azimuth direction shows low correlation in the linear polarization basis. We considered that the scattering mechanisms of the urban areas are the odd- and the even-bounce scattering types and do not satisfy the reflection symmetry except for the area as urban 2. These results support our consideration.

The natural distributed areas show low correlation in the linear and the circular polarization bases due to a property of the reflection symmetry and the volume scattering.

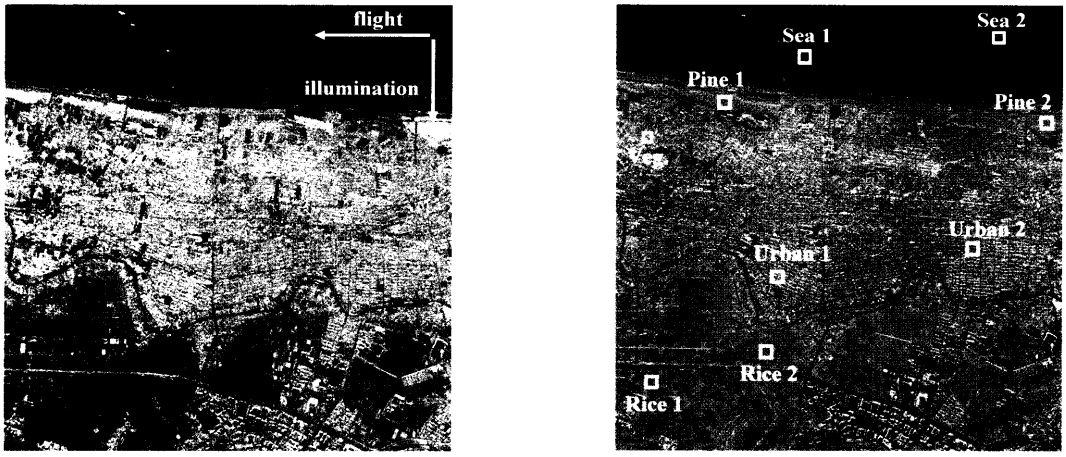

(a) L-band (b) X-band

Fig. 4 The color composite images of Kobari area.

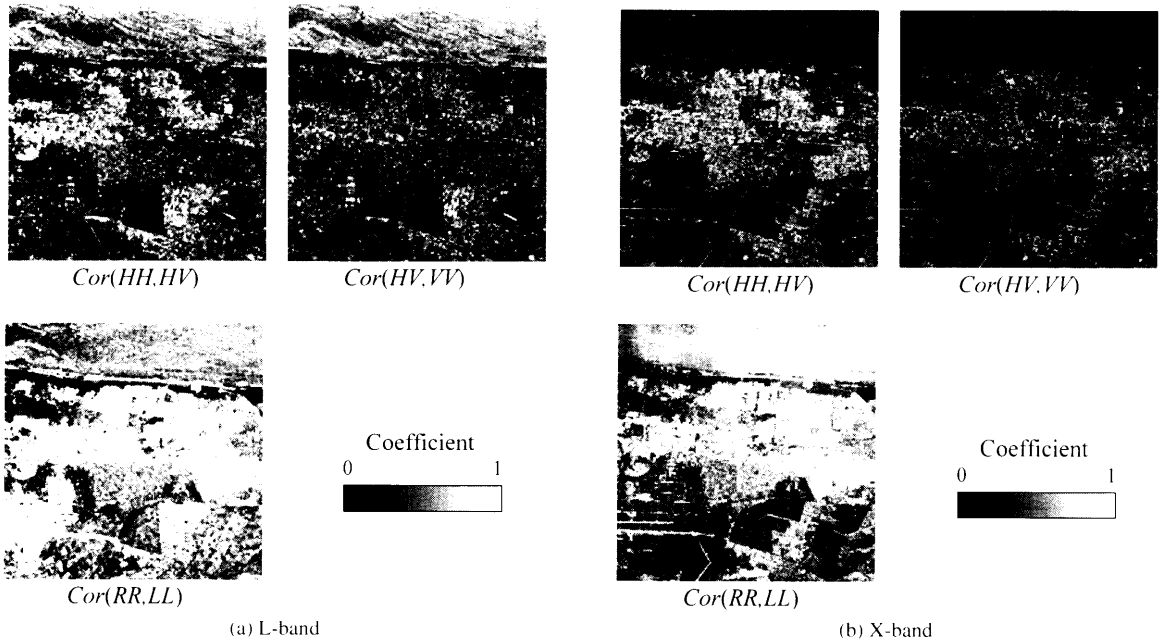

(a) L-band (b) X-band

Fig. 5 The images of three polarimetric correlation coefficients.

NII-Electronic Library Service

Institute of Electronics, Information, and Communication Engineers

Table 2 The magnitude of averaged coefficient in five evaluated areas.

(a) L-band

L-band	Urban areas		Rice paddy areas		Pine woods areas		Sea areas		Vegetable field area
	1	2	1	2	1	2	1	2	
$\|Cor(HH,HV)\|$	0.54	0.22	0.42	0.37	0.17	0.17	0.64	0.50	0.27
$\|Cor(HV,VV)\|$	0.40	0.22	0.20	0.32	0.22	0.17	0.64	0.52	0.24
$\|Cor(RR,LL)\|$	0.67	0.90	0.67	0.94	0.16	0.16	0.66	0.62	0.31

(b) X-band

X-band	Urban areas		Rice paddy areas		Pine woods areas		Sea areas		Vegetable field area
	1	2	1	2	1	2	1	2	
$\|Cor(HH,HV)\|$	0.58	0.19	0.12	0.12	0.15	0.14	0.18	0.24	0.13
$\|Cor(HV,VV)\|$	0.33	0.19	0.11	0.12	0.13	0.13	0.13	0.14	0.12
$\|Cor(RR,LL\|)$	0.63	0.83	0.22	0.27	0.12	0.22	0.86	0.87	0.15

However, $Cor(S_{RR}, S_{LL})$ in the sea area is higher than that in the land distributed areas, because the dominant scattering mechanism of the sea area is the surface scattering, and is different from the volume scattering. In addition, the difference between X-band and L-band appears in the sea area in the linear polarization basis and the neighborhood of the rice 1 area in the circular polarization basis. In the sea area, the scattering mechanism becomes deterministic due to a long wave length of L-band. In rice paddy field area, the double-bounce scattering between a stem of rice and the ground becomes the main scattering mechanism due to a deep penetration capability of L-band, and is interpreted as the cardinal effect of the urban areas.

Therefore, polarimetric features of X-band give us useful information for a detection of the urban areas in the natural distributed areas. However, there are two weaknesses to use X-band data. First, in the linear polarization basis, the polarimetric correlation coefficient between like- and cross-polarized channels cannot be used, when a direction of street pattern is parallel to the azimuth direction. Second is that an increase of angle ϕ of street pattern toward the radar decrease the polarimetric correlation coefficient between *RR* and *LL*. However, it is expected that a combination of the coefficients of the linear and the circular polarization bases compensate for weakness of each coefficient. Moreover, the L-band data showed the complicated scattering mechanisms in comparison with X-band case, and provided a possibility of detailed classification for the natural areas using the polarimetric correlation coefficient.

6. Conclusion

In this paper, we examined the polarimetric correlation coefficients between the linear and the circular polarization bases for feature extraction from multi-frequency POLSAR data. Based on the several polarimetric scattering models, it was found that the coefficient between like- and cross-polarized channels in the linear polarization basis and the coefficient between like-polarized channels in the circular polarization basis become useful index for the discrimination between the urban areas and the natural distributed areas. The experimental results of the X-band showed the usefulness of these coefficients to actual POLSAR data. Moreover, it is possible that the polarimetric correlation coefficient of the L-band improves the detail classification of the natural areas.

References

[1] S.R. Cloude and E. Pottier, "A review of target decomposition theorems in radar polarimetry," IEEE Trans. Geosci. Remote Sens., vol.34, no.2, pp.498–518, March 1996.
[2] S.R. Cloude and E. Pottier, "An entropy based classification scheme for land applications of polarimetric SAR," IEEE Trans. Geosci. Remote Sens., vol.35, no.1, pp.68–78, Jan. 1997.
[3] A. Freeman and S.L. Durden, "A three-component scattering model for polarimetric SAR data," IEEE Trans. Geosci. Remote Sens., vol.36, no.3, pp.963–973, May 1998.
[4] Y. Hara, R.G. Atkins, S.H. Yueh, R.T. Shin, and J.A. Kong, "Application of neural networks to radar image classification," IEEE Trans. Geosci. Remote Sens., vol.32, no.1, pp.100–109, Jan. 1994.
[5] J.-S. Lee, M.R. Grunes, and E. Pottier, "Quantitative comparison of classification capability: Fully polarimetric versus dual and single-polarization SAR," IEEE Trans. Geosci. Remote Sens., vol.39, no.11, pp.2343–2351, Nov. 2001.
[6] F. Mattia, T.L. Toan, J.-C. Souyris, G.D. Carolis, N. Floury, F. Posa, and G. Pasquariello, "The effect of surface roughness on multifrequency polarimetric SAR data," IEEE Trans. Goesci. Remote Sens., vol.35, no.4, pp.954–966, July 1997.
[7] M. Murase, Y. Yamaguchi, and H. Yamada, "Polarimetric correlation coefficient applied to three classification," IEICE Trans. Electron., vol.E84-C, no.12, pp.1835–1840, Dec. 2001.
[8] G. Franceschetti, A. Iodice, and D. Riccio, "A canonical problem in electromagnetic backscattering from buildings," IEEE Trans. Geosci. Remote Sens., vol.40, no.8, pp.1787–1801, Aug. 2002.
[9] T. Moriyama, S. Uratsuka, T. Umehara, H. Maeno, M. Satake, A. Nadai, and K. Nakamura, "Polarimetric SAR image using model fit for urban structures," IEICE Trans. Commun., vol.E88-B, no.3, pp.1234–1243, March 2005.
[10] Y. Dong, B. Forester, and C. Ticehurst, "Radar backscatter analysis for urban environments," Int. J. Remote Sens., vol.18, no.6, pp.1351–1364, 1997.
[11] A. Ishimaru, Wave Propagation and Scattering in Random Media, IEEE Press, 1997.
[12] M. Qong, "A new scattering mechanism enhancement scheme for

NII-Electronic Library Service

Institute of Electronics, Information, and Communication Engineers

polarimetric SAR images," IEEE Trans. Geosci. Remote Sens., vol.40, no.1, pp.2582–2592, Dec. 2002.
[13] Y. Yamaguchi, Fundamentals of Polarimetric Radar and Its Applications, Realize Inc., 1998.
[14] D.G. Micheison and E.V. Jull, "Depolarizing trihedral corner reflectors for radar navigation and remote sensing," IEEE Trans. Antennas Propag., vol.43, no.5, pp.513–518, May 1995.
[15] T. Kobayashi, T. Umehara, M. Satake, A. Nadai, S. Uratsuka, T. Manabe, H. Masuko, M. Shimada, H. Shinohara, H. Tozuka, and M. Miyawaki, "Airborne dual-frequency polarimetric and interferometric SAR," IEICE Trans. Commun., vol.E83-B, no.9, pp.1945–1954, Sept. 2000.

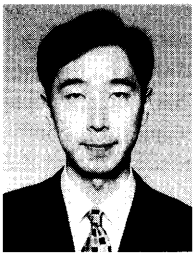

Toshifumi Moriyama was born in Fukui Prefecture, Japan, on January 1, 1972. He received the B.E., M.E. and Ph.D. degrees in Information Engineering from Niigata University, Japan, in 1994, 1995 and 1998, respectively. He was with Fujitsu System Integration Laboratories Ltd. from 1998 to 2003. He is now with the National Institute of Information and Communications Technology. His interests are in the field of radar polarimetry and microwave remote sensing. He is a member of IEEE and Remote Sensing Society of Japan.

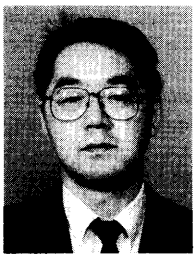

Yoshio Yamaguchi received the B.E. degree in electronics engineering from Niigata University in 1976, and the M.E. and Dr. Eng. Degrees from Tokyo Institute of Technology in 1978 and 1983, respectively. In 1978, he joined the Faculty of Engineering, Niigata University, where he is a professor. From 1988 to 1989, he was a Research Associate at the University of Illinois at Chicago. His interests are in the field of radar polarimetry, microwave sensing and imaging. He has served as Chair of IEEE GRSS Japan Chapter (02-03), vice chair (00-01), organizer of PI-SAR Workshops (00-05) in Japan, and Associate editor for Asian affairs of GRSS Newsletter since 2003. He is a Fellow of IEEE.

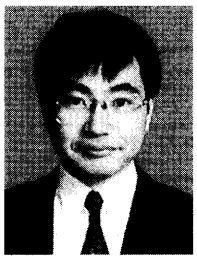

Seiho Uratsuka received the B.S. and M.S. degrees in Geophysics, from Tohoku University, Japan, in 1981 and 1983, respectively. In 1983, he joined the Radio Research Laboratory (now the National Institute of Information and Communications Technology), he has engaged in research in the fields of microwave remote sensing. He received Dr. Eng. degree from Hokkaido University in Applied Physics. He was a guest scientist of Alfred-Wegener-Institute for Polar and Marine Research in Germany from 1992 to 1994. Currently, he is Leader of the Environment Information Technology group, Applied Research and Standards Department, National Institute of Information and Communications Technology. He is a member of IEEE, International Glaciological Society, Remote Sensing Society of Japan and Japanese Society of Snow and Ice.

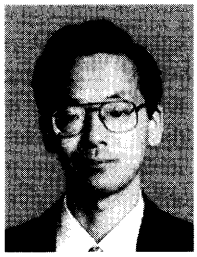

Toshihiko Umehara has been with the National Institute of Information and Communications Technology since 1980. He engaged in study of microwave remote sensing, especially on developing a HF radar, a precipitation radar, an airborne side-looking radar, and an airborne SAR. From 1993 to 1995 he visited the NASA/Goddard Space Flight Center, USA, studying development of the 'Tropical Rainfall Measuring Mission (TRMM) Science Data and Information System' and data processing of rainfall radar. He worked at National Space Development Agency of Japan (NASDA)/Earth Observation Center (EOC), from 1996 to 1998, engaged in developing the NASDA's TRMM Data System. He is now with Applied Research and Standards Department, NICT.

Hideo Maeno graduated Nagoya Kogakuin College of Technology, Nagoya, Japan, in 1980. He received the Ph.D. degree from Chiba University, Japan, in 2003. In 1980, he joined the Radio Research Laboratory (now the National Institute of Information and Communications Technology). He has engaged in research in the fields of radio remote sensing, especially, radar application of the polar ice. Currently, he is working on the imaging radar analysis at the Environment Information Technology Section, Applied Research and Standards Department, National Institute of Information and Communications Technology. He is a member of Remote Sensing Society of Japan and Japanese Society of Snow and Ice.

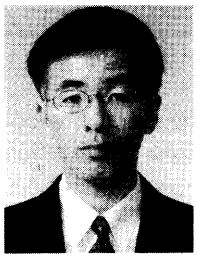

Makoto Satake received the B.E. and M.E. degrees in electrical engineering from Tohoku University, Japan, in 1984 and 1986, respectively. Since 1986 he has been with the National Institute of Information and Communications Technology (NICT), Japan, engaged in study of microwave remote sensing, especially on synthetic aperture radar and rainfall radar. He is now with Applied Research and Standards Department, NICT, primarily working on the calibration of the airborne imaging radar 'PI-SAR' and TRMM Precipitation Radar validation. He is a member of IEEE.

NII-Electronic Library Service

Institute of Electronics, Information, and Communication Engineers

Akitsugu Nadai received the B.S. and M.S. degrees in geophysics from the University of Tokyo in 1989 and 1991, respectively. He joined the National Institute of Information and Communications Technology in the remote sensing since 1991. He engaged in the study on a HF ocean surface radar and an airborne SAR. He is a member of AGU.

Kazuki Nakamura was born in Tokyo, Japan, in January 1974. He received the B.E. in integrated arts and sciences, and the M.E. degree in education from Hokkaido University of Education, Japan, in 1998 and 2000, respectively, and the Ph.D. degree in Science from Chiba University, Japan, in 2003. He joined the National Institute of Information and Communications Technology. His interests are microwave remote sensing of sea and lake ice, and wetland vegetation. He is a member of Remote Sensing Society of Japan and Japanese Society of Snow and Ice.

NII-Electronic Library Service